NTNU

Norwegian University of
Science and Technology

Simulation of pre-rotation in the flow at the inlet of a Reversible Pump Turbine

Kristin Morvik Torød

Master of Energy and Environmental Engineering
Submission date: June 2018
Supervisor: Pål Tore Selbo Storli, EPT
Co-supervisor: Helene Dagsvik, EPT
Jan Tore Billdal, Rainpower

Norwegian University of Science and Technology
Department of Energy and Process Engineering

NTNU
Norwegian University
of Science and Technology

Department of Energy
and Process Engineering

EPT-M-2018-99

MASTER THESIS

for

Student Kristin Torød

Spring 2018

Simulation of pre-rotation in the flow at the inlet of a Reversible Pump Turbine

Simulering av prerotasjon i innløpsstrømningen til en Reversibel Pumpeturbin

Background

Norway has 50% of the European hydro reservoir energy storage, and many of these sites are highly suitable for retrofitting of pump-storage capabilities. The limiting factor for operation is often the phenomena known as cavitation. To avoid this, the units must be submerged, which is an expensive action. The amount of submergence needed is determined by the flow conditions at off-design conditions, and at these conditions there is a large mismatch between the flow angles and angles of the inlet geometry. Adding a rotation to the flow before it enters the inlet of the runner (pre-rotation) might be an effective countermeasure for cavitation, reducing the necessary submergence. Another interesting aspect is if pre-rotation will change the pump characteristic curves, indicating that pre-rotation can be used to control the operation of the pump as well as improving the cavitation properties of the unit.

Objective: Conduct a thorough investigation of the effect of a pre-rotation with respect to characteristics and cavitation, and conclude whether pre-rotation has the desired effect or not for an actual model of a reversible pump turbine runner.

The following tasks are to be considered:

1. Literature review of pump turbine design philosophy and criteria
2. Use the RPT model design for the Francis rig at the Waterpower laboratory to determine the pump characteristics of the model and if possible evaluate the risk of inlet cavitation
3. Investigate if imposed pre-rotation of the flow will affect the characteristic and cavitational properties of the model
4. If the student goes to Nepal for an excursion, earlier and further work will be presented as a publication and presented at the conference; 8th International symposium on Current Research in Hydraulic Turbines (CRHT-VIII) at Kathmandu University in March 2018

-- ” --

Within 14 days of receiving the written text on the master thesis, the candidate shall submit a research plan for his project to the department.

When the thesis is evaluated, emphasis is put on processing of the results, and that they are presented in tabular and/or graphic form in a clear manner, and that they are analyzed carefully.

The thesis should be formulated as a research report with summary both in English and Norwegian, conclusion, literature references, table of contents etc. During the preparation of the text, the candidate should make an effort to produce a well-structured and easily readable report. In order to ease the evaluation of the thesis, it is important that the cross-references are correct. In the making of the report, strong emphasis should be placed on both a thorough discussion of the results and an orderly presentation.

The candidate is requested to initiate and keep close contact with his/her academic supervisor(s) throughout the working period. The candidate must follow the rules and regulations of NTNU as well as passive directions given by the Department of Energy and Process Engineering.

Risk assessment of the candidate's work shall be carried out according to the department's procedures. The risk assessment must be documented and included as part of the final report. Events related to the candidate's work adversely affecting the health, safety or security, must be documented and included as part of the final report. If the documentation on risk assessment represents a large number of pages, the full version is to be submitted electronically to the supervisor and an excerpt is included in the report.

Pursuant to "Regulations concerning the supplementary provisions to the technology study program/Master of Science" at NTNU §20, the Department reserves the permission to utilize all the results and data for teaching and research purposes as well as in future publications.

The final report is to be submitted digitally in DAIM. An executive summary of the thesis including title, student's name, supervisor's name, year, department name, and NTNU's logo and name, shall be submitted to the department as a separate pdf file. Based on an agreement with the supervisor, the final report and other material and documents may be given to the supervisor in digital format.

☐ Work to be done in lab (Water power lab, Fluids engineering lab, Thermal engineering lab)
☐ Field work

Department of Energy and Process Engineering, 15. January 2018

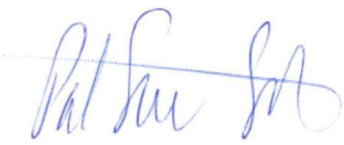

Pål-Tore Storli
Academic Supervisor

Co-supervisor: Helene Dagsvik, Jan Tore Billdal

Abstract

In this master thesis, CFD simulations of an imposed pre-rotation in the flow at the inlet of a reversible pump turbine (RPT) were carried out in ANSYS CFX. The simulations were conducted on the RPT model designed by Olimstad [8] and experimental data from Stranna's [11] measurements were used as boundary conditions. The objective of this thesis is to conduct an investigation of the effect of pre-rotation with respect to cavitation. Adding a rotation to the flow before it enters the inlet of the impeller might be an effective countermeasure for cavitation as it might decrease the presence of low-pressure zones on the blades.

Simulations for three different volume flows, a low volume flow, the volume flow for BEP and a large volume flow, were conducted. The magnitude of the low and large volume flows were 0.4775 and 1.3823 times the flow at BEP, respectively. Pre-rotation was imposed by adding a rotational velocity component to the flow at the inlet, and simulations with a rotational velocity component of 16 different magnitudes were carried out for every volume flow. In total 48 simulations were conducted and compared with each other. First, the 16 simulations with the same volume flow and different rotational components were compared with each other, and then the trends found for the three different volume flows were compared.

The area of the low-pressure zones decreased for all volume flows when more pre-rotation was added. As the flow develops from the inlet of the domain to the inlet of the blade the magnitude of the rotational component of the velocity as it approaches the blade is unknown. The way the pre-rotation in the flow at the inlet was imposed was not optimal and this contributes to a development of the rotational velocity as well. Because of this, the direct relation between the actual magnitude of the imposed pre-rotation and the decrease in the area of the low-pressure zones can not be evaluated in this master thesis.

Sammendrag

I denne masteroppgaven ble det gjennomført CFD-simuleringer av prerotasjon i innløpsstrømningen til en Reversibel Pumpeturbin i simuleringsverktøyet ANSYS CFX. Simuleringer av RPT-modellen designet av Olimstad [8] ble utført og eksperimentelle data fra Stranna [11] sine målinger ble brukt som grensebetingelser. Hensikten med denne masteroppgaven er å undersøke effekten av prerotasjon med hensyn til kavitasjon. Å påføre rotasjon til strømningen før den entrer innløpet til impelleren kan være et effektivt mottiltak mot kavitasjon fordi prerotasjonen kan muligens bidra til å redusere arealet av områder med lavt trykk.

Simuleringene ble gjennomført for tre ulike volumstrømmer, en lav, en for BEP og en høy. Prerotasjon ble påført ved å legge til en roterende hastighetskomponent til strømningen ved innløpet, og simuleringer med 16 forskjellige roterende hastighetskomponenter ble gjennomført for hver volumstrøm. Totalt ble 48 forskjellige simuleringer gjennomført og sammenliknet med hverandre. De 16 simuleringene med lik volumstrømning ble først sammenliknet med hverandre og så ble trendene for de tre volumstrømningene sammenliknet.

For alle volumstrømmene minket arealet til områdene med lavt trykk når mer prerotasjon ble påført. Fordi strømningen utvikler seg fra innløpet til domenet til bladet vil størrelsen til den roterende hastighetskomponenten være ukjent ved innløpet til bladet. Måten prerotasjonen er påført er ikke optimal og dette birdar også til at den roterende hastighetskomponenten utvikler seg. På grunn av denne utviklingen kan ikke en direkte sammenheng mellom størrelsen til den roterende hastighetskomponenten og reduskjonen av arealet med lavt trykk evalueres i denne masteroppgaven.

Preface

I would like to thank my supervisor Pål-Tore Storli for helpful guidance and Petter Østby and Chirag Trivedi for useful input regarding my simulations. I would also like to thank everybody at the Waterpower Laboratory for creating a friendly and open environment where it is easy to ask for help and where people are interested in discussing problems one may encounter while writing a master thesis.

Kristin Morvik Torød, 14.06.18

Table of Contents

List of Tables

List of Figures

Nomenclature

Symbols

Symbol	Description	Unit
$NPSH$	Net Positive Suction Head	m
u	Peripheral Velocity	m/s
c_u	Peripheral Absolute Velocity Component	m/s
c_m	Meridional Absolute Velocity Component	m/s
w_u	Peripheral Relative Velocity component	m/s
β	Blade Angle	[degree]
ω	Rotational Speed	$1/s$
n	Rotational Speed	rpm
η	Efficiency	$\%$
Q	Flow Rate	kg/m^3
H	Head	m
ρ	Density	kg/m^3
p	Pressure	Pa
g	Acceleration of gravity	m/s
r	Radius	m
D	Diameter	m
B	Impeller Height	m
A	Area	m^2
v	Velocity	m/s
h	Height	m

Subscript

Symbol	Description
0	Domain inlet
1	Pump/impeller inlet
2	Pump outlet

Abbreviations

Symbol	Description
RPT	Reversible Pump Turbine
CFD	Computational Fluid Dynamics
BEP	Best Efficiency Point
SST	Shear Stress Transport
LES	Large Eddy Simulations
DNS	Direct Numerical Simulations
RMS	Root Mean Square

Chapter 1

Introduction

A reversible pump turbine (RPT) is a combination of a Francis turbine and a centrifugal pump, and can therefore operate both as a turbine and as a pump [12] [13]. This double characteristic enables the RPTs to play an important role in the future of hydropower. As new intermittent energy sources constitute a larger and larger part of the energy mixture it is crucial to stabilize the electric power system. Pumped hydro storage power plants are an efficient solution as they can boost production and consumption in peak power situations when operated in turbine or pump mode, respectively. Depending on reservoir size, pumped hydro storage power plants can also deliver long term energy storage [8]. Preliminary work for this master thesis is conducted in Torøds project thesis where pump turbine design philosophy and criteria are reviewed and the pump characteristics of the RPT model at the Waterpower Laboratory are determined [13].

A limiting factor for operation of an RPT is cavitation. In a pump the local pressure can fall below the vapour pressure for the pumped liquid. Thus, bubbles of vapour, called cavitation bubbles, will appear. This will typically occur on the suction side of the impeller blades where the pressure is lowest, and the flow will transport the cavitation bubbles to regions with higher pressure where they collapse. It is the collapse of cavitation bubbles that is undesirable as it causes vibration, noise, reduction in efficiency, and damage to the impeller blades [4].

To avoid cavitation the local pressure everywhere inside the pump must be above the vapour pressure. This is ensured by submerging the pump below the required Net Positive Suction Head, $NPSH_r$. $NPSH_r$ is defined as the minimum $NPSH$ necessary to avoid cavitation in the pump, where $NPSH$ is defined as the difference between the inlet stagnation pressure head in the pump and the vapour pressure head [4].

$NPSH_r$ is lowest when the pump works at design conditions, and increases for operational points further away from the design point, as shown by the lowest graph in Figure 1.1. It is therefore desirable to investigate how to decrease $NPSH_r$ at off-design conditions in order to extend the operational range for the pump. Such a decrease will straighten and extend the bottom part of the submergence graph, Figure 1.1 [13]. It is assumed that the reason for the rapid increase in $NPSH_r$ is that the difference between the inlet flow angle and the geometry of the impeller increases enough for allowing local low-pressure zones to appear. The objective of this thesis is to conduct an investigation of the effect of pre-rotation with respect to cavitation. Adding a rotation

to the flow before it enters the inlet of the runner might be an effective countermeasure for cavitation, reducing the necessary submergence. The rationale for this is explained in section 2.2.

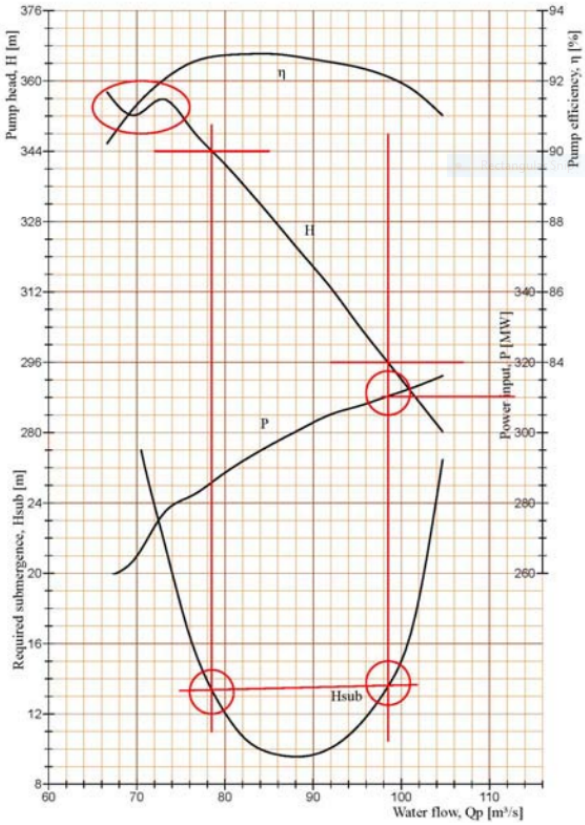

Figure 1.1: Pump performance diagram with critical points [1].

Chapter 2

Theory

2.1 Velocity triangles

The velocity triangles in Figure 2.1 show the correlation between the velocity components at the inlet and outlet of an RPT [2] [3]. For a centrifugal pump with no pre-rotation at the inlet flow the value of c_{u1} is zero [10].

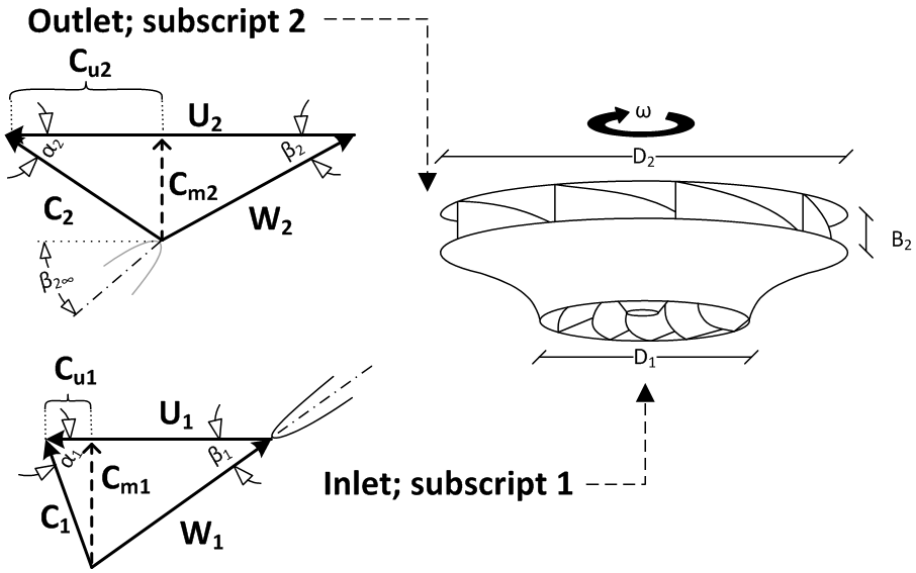

Figure 2.1: Velocity triangles at the inlet and outlet of an RPT.

The peripheral velocity at the inlet, u_1, is a function of the inlet radius and the rotational speed as shown in Equation 2.1, and the meridional component of the absolute velocity at the inlet, c_{m1}, is a function of the inlet area and the volume flow as shown in Equation 2.2. The inlet blade angle, β_1, is constant, and all the other unknowns of the inlet velocity triangle can be computed from

these three values.

$$u_1 = r_1\omega \tag{2.1}$$

$$c_{m1} = \frac{Q}{A_1} \tag{2.2}$$

2.2 Pre-rotation

When pre-rotation is imposed upon the inlet flow of the impeller, the value of c_{u1} is no longer zero. Equation 2.3 can be deduced from the geometrical correlations between the inlet velocity components [3].

$$c_{u1} = u_1 - w_{u1} = u_1 - \frac{c_{m1}}{\tan\beta_1} = r_1\omega - \frac{Q}{A_1 \tan\beta_1} \tag{2.3}$$

For a constant rotational speed, the volume flow is the only variable affecting the size of c_{u1}. Figure 2.2a shows the velocity triangle at the inlet for BEP.

Figure 2.2b and 2.2c show respectively the velocity triangles at the inlet for volume flows smaller and larger than the flow for BEP.

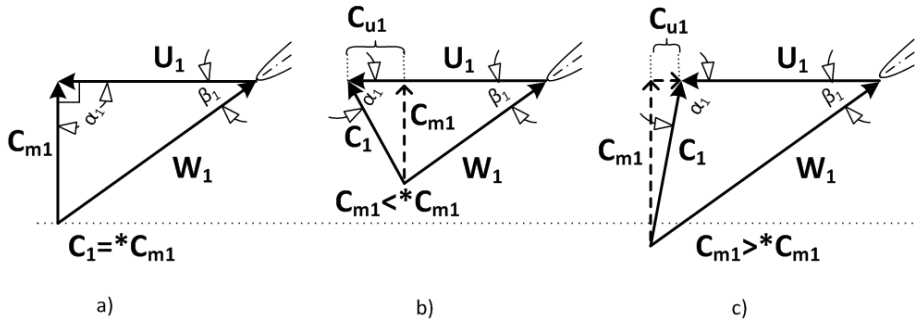

Figure 2.2: Inlet velocity triangles for a centrifugal pump.

The velocity triangles in Figure 2.2 shows the size and direction of the velocity components as the flow hits the impeller. In all figures the relative velocity is perfectly aligned with the direction of the impeller blade. In reality the direction of the relative velocity will differ from the direction of the blade.

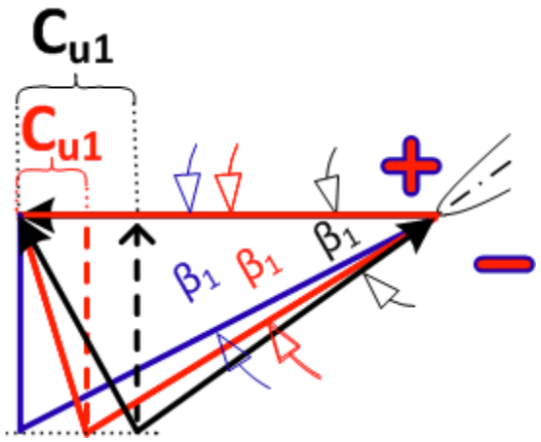

Figure 2.3: Inlet velocity triangles with varying c_{u1}.

For a discharge smaller than the design discharge, as in Figure 2.2b and the black triangle in Figure 2.3, the flow must have a certain rotational component in order to align perfectly with the direction of the blade. If there is no device in front of the inlet adding the necessary angular momentum to the flow to obtain this rotational component, the flow will approach the inlet with $\alpha_1 = 90^o$, like the blue triangle in Figure 2.3. This causes a mismatch between the flow angle and the blade angle, referred to as the angle of attack.

The side of the blade that hits the flow at the inlet is called the pressure side and the other side of the blade is called the suction side. On the pressure side there is a high pressure and a low velocity and on the suction side the pressure is low and the velocity is high [2]. The pressure difference on the pressure- and suction side of the blade is indicated by the red and blue plus and minus signs in figure 2.3. When the flow approaches the inlet this pressure difference gives momentum to the fluid, which results in a rotational component of the flow. This reduces the mismatch between the flow angle and the blade angle and the inlet velocity triangle will look more like the red velocity triangle in Figure 2.3.

As long as the initial flow angle is smaller than the blade angle the flow will hit the blade on the pressure side, increasing the already existing pressure difference on the pressure- and suction side of the blade. It is the presence of the low pressure region that can initialize cavitation, if the pressure is low enough [4]. This is the reason an imposed pre-rotation in the flow at the inlet is believed to counteract the formation of low pressure regions, as it might cause the velocity triangle to shift towards the black velocity triangles in Figure 2.2 and 2.3.

Adding pre-rotation in the flow at the inlet is not a new measure to counteract cavitation. It is common for centrifugal pumps to operate in conjunction with inducers. An inducer is an axial flow impeller and serves as a booster pump for the centrifugal pump. It adds sufficient head to the liquid so that the $NPSH_r$ for the pump is decreased [5].

2.3 Vortex motion

Water that moves in a circular path is known as a vortex motion [10]. Stream cylinders are formed by particles of liquid that describe circles of the same radius, and these particles move with the same tangential and angular velocity. Variation in the linear or angular velocity determines the pressure distribution along the radius if the vessel containing the liquid is not open to the atmosphere. For equilibrium, the centrifugal force must be balanced by the pressure for each particle at the same point, described by Equation 2.4.

$$\frac{dp}{dr} = \frac{\rho}{g}\frac{v^2}{r} = \frac{\rho}{g}\omega^2 r \tag{2.4}$$

Special cases of vortex motion are the free and the forced vortex. Figure 2.4 shows the velocity vectors for some of the fluid particles in these cases. The radial component of the velocity is zero for both the free and the forced vortex, hence the streamlines are circles about the origin, [4]. The free vortex is irrotational, implying that the vorticity is zero everywhere except at the origin. The forced vortex is rotational, which means that the fluid particles rotate as they revolve around the origin.

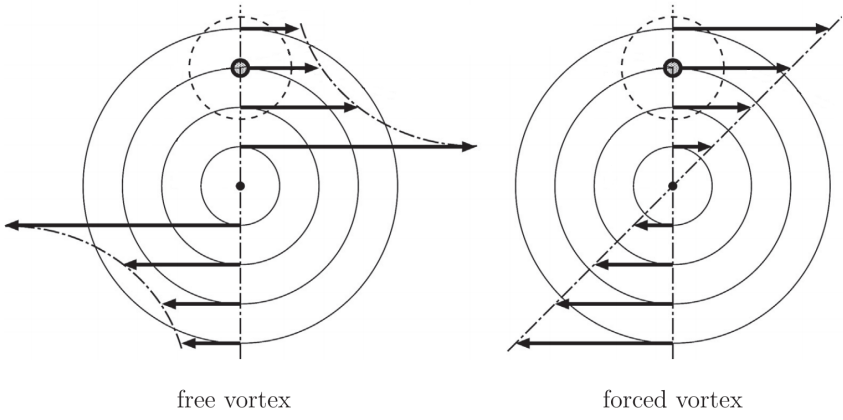

Figure 2.4: Schematics of the free and forced vortices, modified from [6].

For a forced vortex the angular velocity, ω, is constant and the fluid rotates as a solid body. The peripheral velocity increases linearly with the radius, as described by Equation 2.1 and the equation for the pressure distribution, Equation 2.4, is reduced to Equation 2.5.

$$\frac{p}{\rho} = \frac{v^2}{2g} + h \tag{2.5}$$

The vortex motion found at the inlet of an RPT is a version of the forced vortex, but due to the non-rotating walls it will not look exactly like the forced vortex in Figure 2.4. As for the forced vortex, the velocity will increase when the distance from the origin increases, but closer to the wall the velocity will start to decrease and at the wall the velocity will be zero.

2.4 Experimental data

At the Waterpower Laboratory at NTNU there is an RPT designed by Olimstad [8]. Stranna [11] has performed measurements on Olimstad's RPT in pumping mode. In Table 2.1 the geometrical constants for the RPT is presented. In addition, the gravitational constant, g, is set to be $9.81m^2/s$.

Table 2.1: Known constant properties for Olimstad's RPT [9].

Constant	$D_1[m]$	$D_2[m]$	$B_2[m]$	$\beta_1[degree]$	$\beta_{2\infty}[degree]$
Value	0.349	0.6305	0.0587	12.8	12.02

A pre-meshed computer model of the RPT designed by Olimstad is used to conduct the simulations discussed in this master's thesis. The model has the same geometrical properties as the physical RPT. The physical RPT has six blades and when operated in pump mode at 560 rpm, the volume flow at best operation point, Q^*, is $0.1303m^3/s$ and the head at best operation point, H^*, is $17.5065m$.

From Stranna's measurements the volume flow, Q, the outlet pressure, p_2, and the efficiency, η, are extracted for different values of the rotational velocity, n. There are data sets for 10 different rotational velocities, and data for 15-19 different volume flows have been measured for each rotational velocity [13]. For every Q there exists 43 individual data sets. The average values for each Q for all the different rotational velocities are calculated and the corresponding c_{m1}-value is calculated.

The c_{m1}-value and the p_2-value found by evaluating Stranna's data are used as boundary conditions for the simulations. Simulations with an imposed pre-rotation of increasing magnitude are compared to each other and to simulations with no imposed pre-rotation in order to investigate the effect of pre-rotation with respect to cavitation.

Chapter 3

Setup

3.1 Domain

CFD simulations of the RPT designed by Olimstad were carried out in ANSYS CFX in order to investigate whether and how an imposed pre-rotation affects the characteristics and cavitational properties of an RPT. The simulation domain represents only one sixth of the total RPT due to computational costs. The RPT consists of six self-similar blades, and the solution for one blade can therefore be transferred to the other blades as well. The meshed part of Figure 3.1a shows the rotating part of the domain, and the meshed part of Figure 3.1b shows the original inlet, the outlet and the blade. The whole domain is defined as a rotating fluid domain with water as the defined fluid and a rotational velocity of 560 rpm. Since the whole domain is defined as rotating, the upstream and downstream part of the hub and shroud are defined as counter rotating in order to represent stationary walls. The water is defined as a continuous and non-buoyant fluid, set to be isothermal with a temperature of 298.15K. The reference pressure for the domain is 0Pa and the turbulence model is SST, shear stress transport. As can be seen from the coordinate system in Figure 3.1 the flow moves in the z-direction at the inlet.

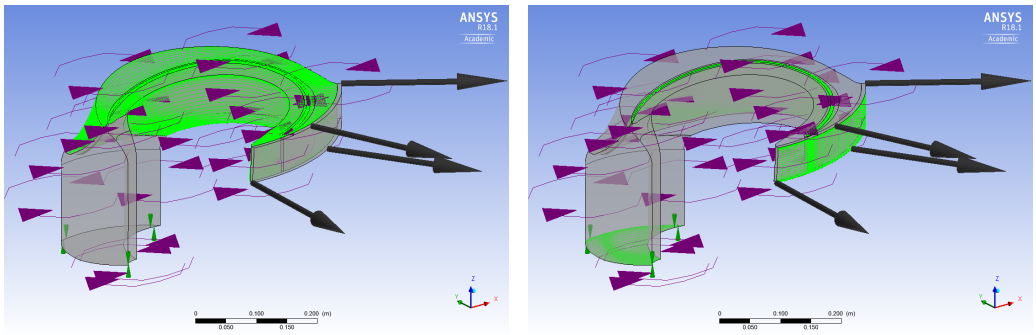

(a) Rotating. **(b)** Inlet outlet blade.

Figure 3.1: Original domain.

The mesh consists of 322048 hexahedrons and 347556 nodes. Figure 3.2 depicts the mesh on the blade. Table 3.1 presents the values for y+ on the blade for the different volume flows. The values presented are rounded averages from all the simulations.

Table 3.1: Yplus

	Low volume flow	BEP	Large volume flow
Min	0.5	0.6	1.4
Max	61	94	113
Avg	13	20	25

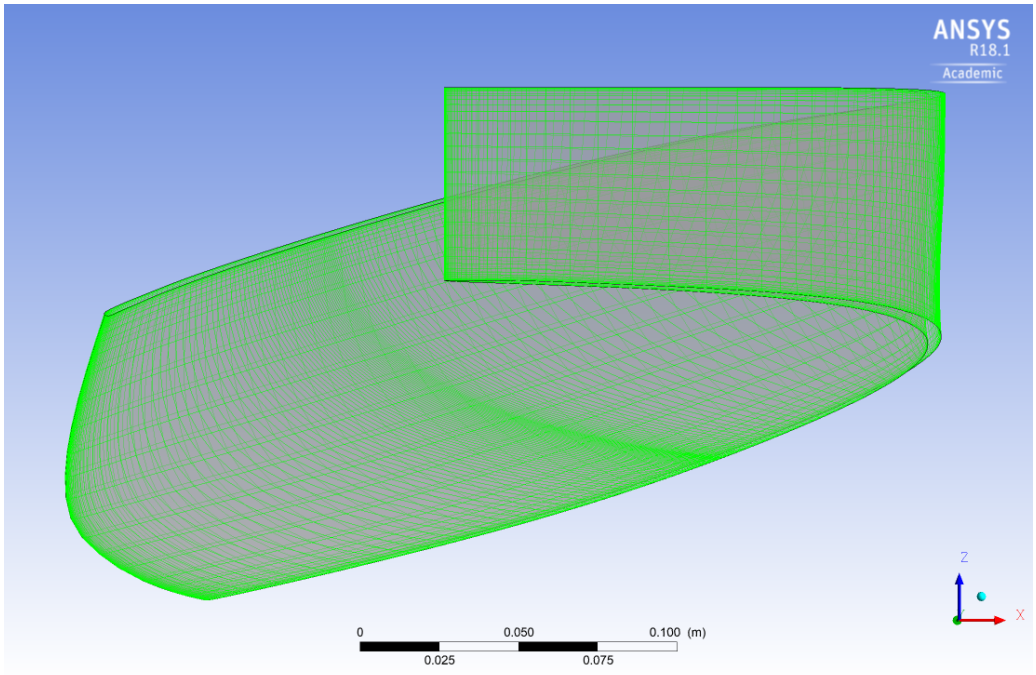

Figure 3.2: Mesh on the blade.

3.2 Inlet

The pre-rotation is imposed on the flow at the inlet of the RPT, but the inlet on the original domain is not far enough from the blade for the flow to be fully developed when it reaches the blade. Because of this the inlet is extended as shown in Figure 3.3a. The extended part of the inlet is $3.5188m$ and the mesh consists of 480000 hexahedrons and 505263 nodes, the length of the original inlet is $0.1336m$. As the new part of the domain is just an extension of the existing geometry a general connection interface model is imposed on the transition between the original and the new part of the domain. The location of this connection is shown in figure 3.3b.

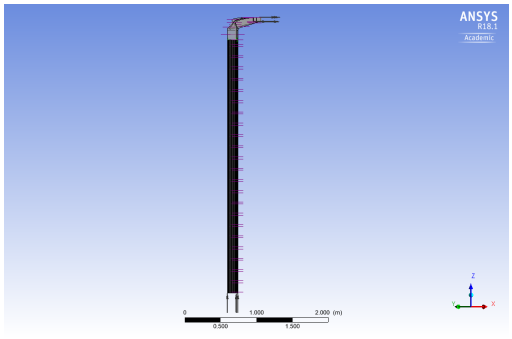

(a) Whole domain.

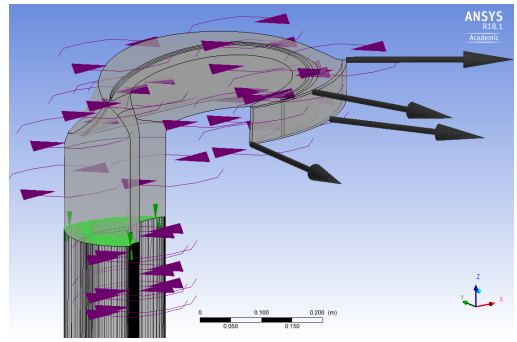

(b) Connection.

Figure 3.3: Simulation domain.

The mesh at the inlet domain is designed to be as similar to the original mesh as possible in order to reduce the impact the connection between the original inlet and the extension has on the flow. Figure 3.4a shows the original mesh at the location of the connection and Figure 3.4b shows the new mesh. The meshes are similar, but not identical. Connection side 1 is the mesh that belongs to the extended inlet, and connection side 2 is the mesh that belongs to the inlet of the original domain, for further reference.

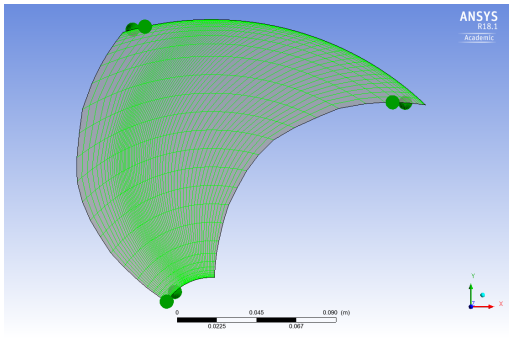

(a) Original mesh, connection side 2.

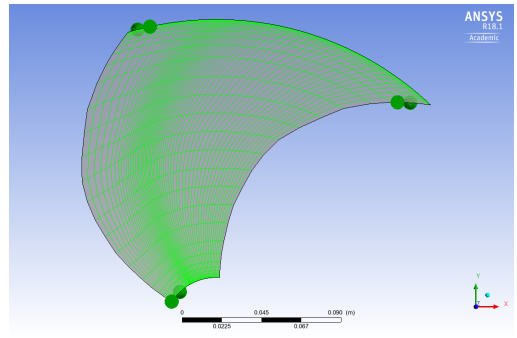

(b) Mesh at the extended inlet, connection side 1.

Figure 3.4: Mesh at the connection

3.3 Boundary conditions

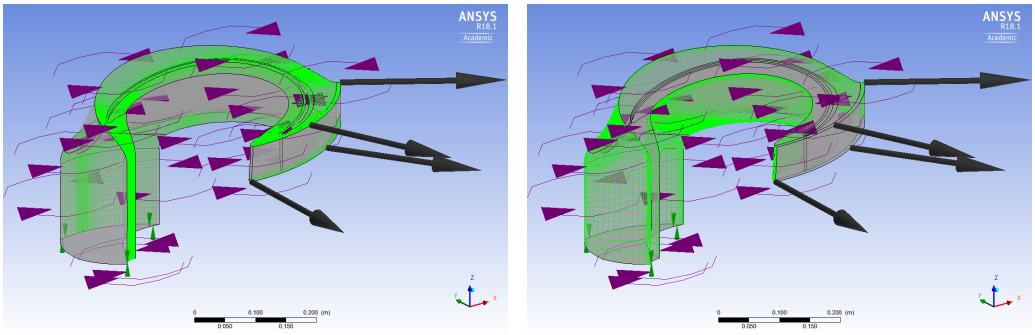

(a) Hub and shroud.

(b) Rotational periodicity.

Figure 3.5: Domain with boundary conditions.

A set of different boundary conditions are defined for the RPT geometry. A smooth no-slip wall boundary is imposed on the blade as well as on the hub and the shroud. On the sides connecting the hub and the shroud, the meshed surfaces in Figure 3.5b, a rotating periodicity boundary condition is imposed. This is done to imitate a simulation of the whole impeller as the flow that moves out of one side comes back in on the other.

The inlet has an inlet boundary type with a subsonic flow regime. *Cartesian Velocity Components* define the boundary condition for mass and momentum. The component of the flow in y-direction is zero for all simulations and the component of the flow in z-direction, c_m, is found by evaluating Stranna's measurements. When Q is kept constant, c_m is also kept constant as c_m is a function of the mass flow and the area alone. Hence, the component of the flow in x-direction, c_u, is the only velocity component that is changing when pre-rotation is imposed on a flow with a constant mass flow rate. The c_u imposed is constant over the whole inlet.

An outlet boundary type is imposed on the outlet of the domain. The flow regime is subsonic, and the boundary condition for mass and momentum is *Average Static Pressure*. The relative pressure imposed is the outlet pressure found by Stranna, and in order to represent the experimental data the pressure averaging is *circumferential* as the measurements were conducted by the outlet wall.

According to Stranna's measurements the volume flow for BEP when $n = 560rpm$ is $0.13029m^3/s$. In order to evaluate the effect of pre-rotation for different operation points, simulations for both BEP, a large volume flow and a low volume flow are carried out. Table 3.2 presents the three different volume flows that were evaluated and the corresponding c_{m1}-values and p_2-values.

Table 3.2: Evaluated volume flows with corresponding c_{m1} and p_2.

$Q[m^3/s]$	$c_{m1}[m/s]$	$p_2[Pa]$
0.06221	0.650301	98557.3
0.13029	1.36199	101326.0
0.18011	1.88274	98940.8

Pre-rotation is imposed by varying the c_u-component of the flow at the inlet, denoted c_{u0}. Subscript 0 is used at the inlet of the domain while subscript 1 is used to describe the geometry at the inlet of the blade. For the three different volume flows the β-angle for $c_{u0} = 0$ is found. β_0 is then increased linearly in such a manner that seven of the β_0-angles are smaller than β_1, one β_0-angle is equal to β_1 and seven β_0-angles are larger than β_1. Equation 3.1 shows the mathematical approach for this.

$$\beta_0^n = \Delta\beta + \beta_0^{n-1} \tag{3.1}$$

Superscript 1 denotes the simulations with no imposed pre-rotation and superscript 8 denotes the simulations where $\beta_0 = \beta_1$. As an extra test a simulation with β_0^{16} = $20 * \Delta\beta$ + β_0^{15} is conducted. Table 3.3, 3.4 and 3.5 presents the different values for β_0 and the corresponding c_{u0}-values imposed on the inlet flow to study the effect pre-rotation has on cavitation. There are no experimental values for p_2 when pre-rotation is imposed, and p_2 is therefore kept constant for every Q.

Table 3.3: Low volume flow. c_{m0} = 0.650301 m/s, $\Delta\beta$ = 1.3091 deg.

n	$\beta_0[rad]$	$\beta_0[deg]$	$c_{u0}[m/s]$
1	0.063463	3.6361	0
2	0.086311	4.9453	-2.71756
3	0.109160	6.2544	-4.29956
4	0.132008	7.5635	-5.33564
5	0.154857	8.8726	-6.06746
6	0.177705	10.1818	-6.61238
7	0.200554	11.4909	-7.03428
8	0.223402	12.8000	-7.37090
9	0.246251	14.1091	-7.64600
10	0.269099	15.4182	-7.87524
11	0.291948	16.7274	-8.06940
12	0.314796	18.0365	-8.23612
13	0.337645	19.3456	-8.38097
14	0.360493	20.6547	-8.50812
15	0.383342	21.9639	-8.62073
16	0.840311	48.1463	-9.65068

Table 3.4: BEP. c_{m0} = 1.36199 m/s, $\Delta\beta$ = 0.7455 deg.

n	$\beta_0[rad]$	$\beta_0[deg]$	$c_{u0}[m/s]$
1	0.132317	7.5812	0
2	0.145329	8.3267	-0.927554
3	0.158341	9.0723	-1.70364
4	0.171353	9.8178	-2.36276
5	0.184366	10.5634	-2.92969
6	0.197378	11.3089	-3.42266
7	0.210390	12.0545	-3.85539
8	0.223402	12.8000	-4.23841
9	0.236414	13.5455	-4.57993
10	0.249426	14.2911	-4.88645
11	0.262439	15.0366	-5.16318
12	0.275451	15.7822	-5.41433
13	0.288463	16.5277	-5.64338
14	0.301475	17.2733	-5.85318
15	0.314487	18.0188	-6.04613
16	0.574731	32.9296	-8.13029

Table 3.5: High volume flow. c_{m0} = 1.88274 m/s, $\Delta\beta$ = 0.3393 deg.

n	$\beta_0[rad]$	$\beta_0[deg]$	$c_{u0}[m/s]$
1	0.181948	10.4249	0
2	0.187870	10.7642	-0.329917
3	0.193792	11.1035	-0.639902
4	0.199714	11.4428	-0.931726
5	0.205636	11.7821	-1.20696
6	0.211558	12.1214	-1.46700
7	0.217480	12.4607	-1.71308
8	0.223402	12.8000	-1.94631
9	0.229324	13.1393	-2.16770
10	0.235246	13.4786	-2.37813
11	0.241168	13.8179	-2.57841
12	0.247090	14.1572	-2.76928
13	0.253012	14.4965	-2.95139
14	0.258934	14.8358	-3.12534
15	0.264856	15.1751	-3.29168
16	0.383296	21.9612	-5.56418

3.4 Uncertainties in the simulation model

When doing CFD simulations several uncertainties have to be properly accounted for in order to get reliable results.

Domain
The CFD simulations were only conducted on the impeller and not the whole RPT. The omitted parts might have either a small or a major impact on the flow, but that was not taken into consideration for these simulations.

Mesh
The original domain was provided as a pre-meshed .cgns file without any possibilities of changing the mesh. It was therefore not possible to conduct a mesh refinement study. Such a study requires at least three different meshes to be compared in order to investigate whether the used mesh is fine enough for the simulations to converge towards the same results as a finer mesh. In the worst case scenario the mesh may be too coarse for the simulations to give an accurate result.

Steady state
In this master's thesis no attention is paid to pulsations of any kind, hence only steady state simulations are performed. A steady state simulation is only reliable once it has converged, and the result are not time dependent. Due to the lack of time dependency no time step was defined and no time step refinement study has to be conducted.

Mass conservation
Mass conservation was checked by comparing the mass flow at the inlet with the mass flow at the outlet. The error was estimated to be below 0.3% for all the simulations at BEP and below 0.04% for all the simulations with a large volume flow. For one of the simulations with a low volume flow the mass conservation error was estimated to be 3.3%, and for the rest of the simulations with a low volume flow the error was estimated to be below 0.32%.

Turbulence model
The SST model simple and widely used for turbomachinery simulations. It is a combination of the best parts of the $k-\omega$-model and the $k-\epsilon$-model, but as all models it is not able to give a completely accurate description of the reality [7]. More accurate results can be conducted with LES (large eddy simulations) or DNS (direct numerical simulations), but these kind of simulations takes a lot of time and are therefore avoided if the results given by using a turbulence model are good enough.

Convergence

The convergence criterion for the simulations was set to be of max residual type with a residual target of 0.0001. This criterion was never met for any of the simulations and all the simulations were stopped after 300 iterations. As the rotating speed of the impeller was 560 rpm and the physical timescale was 1/560, 300 iterations corresponds to 5 rotations of the impeller. The RMS-values for mass and momentum did not converge towards one constant value, but fluctuated periodically. In Torøds project thesis [13] some of the simulations went on for 1120 iterations and as they did not converge any further, 300 iterations were deemed sufficient for the simulations. The convergence of the RMS-values for mass and momentum at BEP with no imposed pre-rotation are visualized in Figure 3.6.

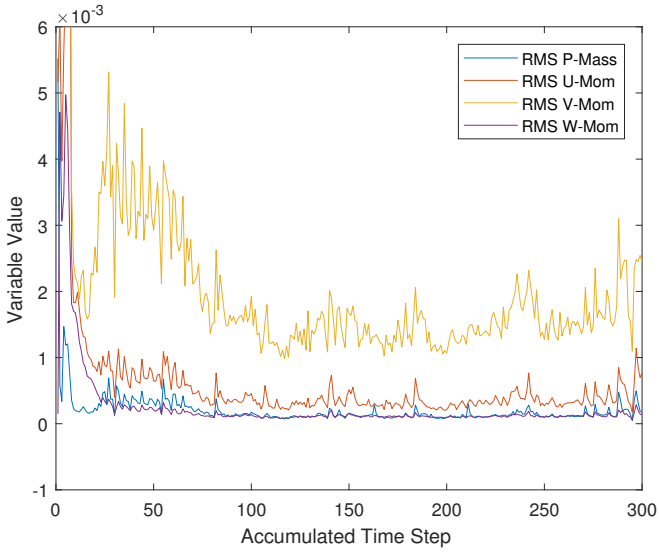

Figure 3.6: Convergence of the RMS-values for mass and momentum when $c_{m0} = 1.36199 m/s$ and $c_{u0} = 0 m/s$.

Walls on the inlet part of the domain

On the inlet part of the domain two walls were defined as an extension of the hub and the shroud. The outer wall is forming the wall boundary of the tube the water is flowing within, while the inner wall boundary implies that the shaft the impeller is rotating around is extended further down in the inlet of the RPT. This is not the case for the real model and can lead to inaccuracies in the simulations.

Chapter 4

Results and Discussion

After running the 48 simulations the pressure on the blade was evaluated for all the cases. Figure 4.1, 4.2 and 4.3 show respectively the results for simulations with low volume flow, volume flow at BEP and large volume flow. On the y-axis the pressure is given in kilopascal and on the x-axis the area of the blade is given in percent. The curves are cumulative, which means that for a given simulation and pressure the corresponding area represents the area on the blade with a pressure equal to or lower than the given pressure. As an example does 6.11 % of the area of the blade have a pressure lower than -50000 Pa in the simulation where $c_{m0} = 0.650301$ m/s and $c_{u0} = 0m/s$, the green line in Figure 4.1. The total area of the blade is 0.123515 m^2. In Figure 4.2 and 4.3 the graphs start to deviate from the trend when the area of the low pressure zones cover less than 0.1 % of the total area. One of the factors that may be the reason for this is inaccuracy due to the decreasing difference in the size of the low pressure zones and the size of the mesh elements. In the discussion only the clear trend is taken into consideration, not the deviations that occur for small areas.

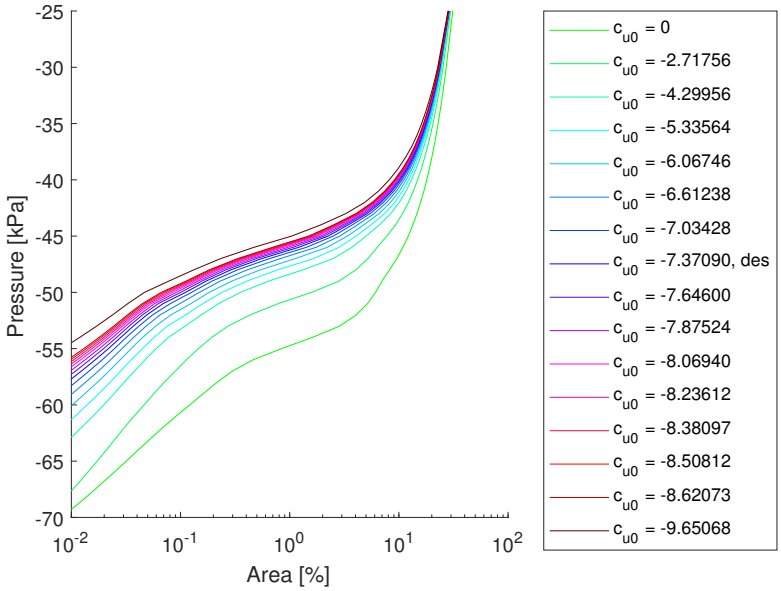

Figure 4.1: Low volume flow. c_{m0} = 0.650301 m/s, p_2 = 98557.3 Pa

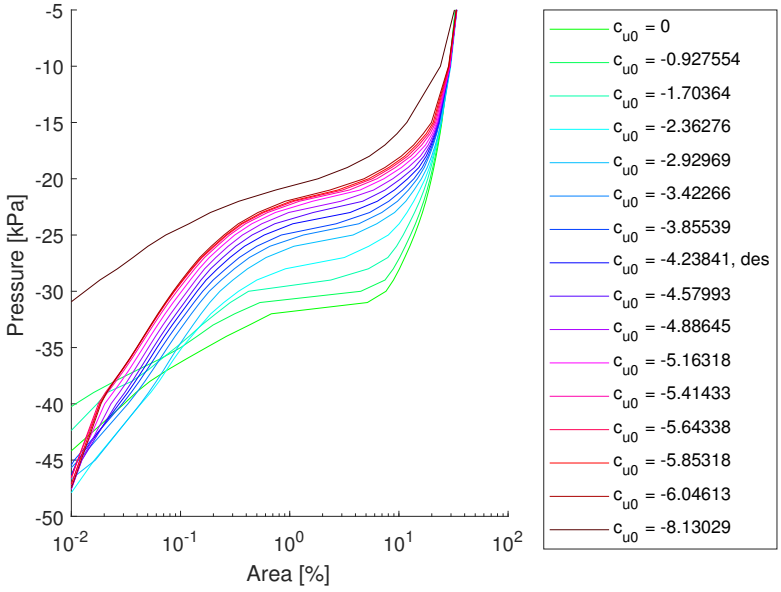

Figure 4.2: BEP. c_{m0} = 1.36199 m/s, p_2 = 101326 Pa

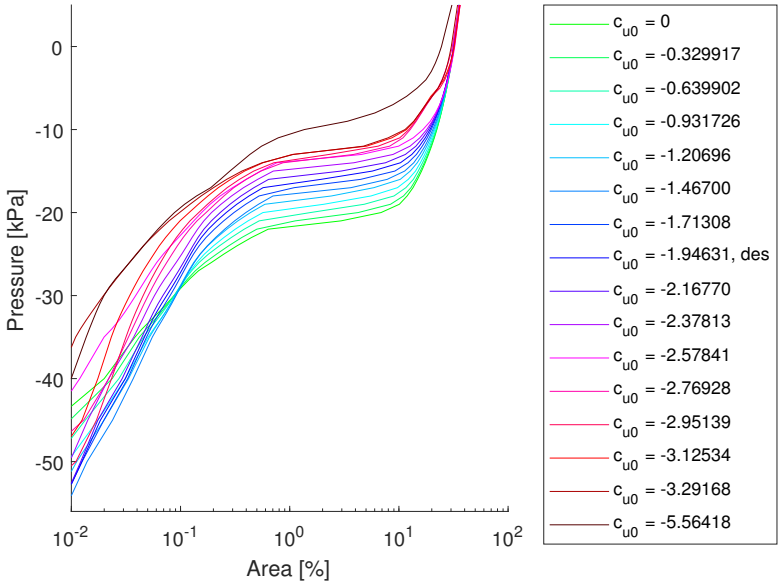

Figure 4.3: High volume flow. c_{m0} = 1.88274 m/s, p_2 = 98940.8 Pa

From the results it is evident that for all the simulations the pressure on a large part of the blade is negative. The imposed pressure at the outlet corresponds to experimental values, but the domain pressure which is set to be 0 Pa does not and that is probably the reason why negative pressure zones appear. Negative pressure zones are not physical as there is no such thing as negative pressure. Although, they are not necessarily a problem here as the simulations are only compared with each other and not with experimental data. The main concern in this thesis is to evaluate how an imposed pre-rotation affects the pressure zones, and that is possible even if the numerical solution for the pressure is unphysical. In contrast to the numerical solution for the pressure, the development of the pressure zones can be physical.

For all the volume flows the simulations show the same trend. The area of the low pressure regions decreases as more pre-rotation is imposed. It also looks like the decrease happens more rapidly for the low volume flow, Figure 4.1, while it is almost linear for the high volume flow, Figure 4.3,. However, as $\Delta\beta$ is larger for the low volume flow, the three graphs cannot be directly compared to each other. In all three figures the difference between the graph for c_{u0}^{16} and the graph for c_{u0}^{15} is smaller than the difference difference between the graph for c_{u0}^{15} and the graph for c_{u0}^{1}, which implies that the low pressure zones do not decrease linearly for any of the volume flows.

Usually $\beta_0 = \beta_1$ for BEP, $\beta_0 < \beta_1$ for a volume flow less than the volume flow for BEP and, $\beta_0 > \beta_1$ for a volume flow larger than the volume flow for BEP. In this master thesis however, $\beta_0 < \beta_1$ for all the considered volume flows. Design point for a centrifugal pump is normally at its best efficiency point, but as Olimstads RPT is designed for turbine mode the design point in pump mode might be different from BEP in pump mode. The RPT is also designed to be unstable in turbine mode as it is made for research purposes so it is expected that the behaviour is not optimal. The inlet of the blade of the RPT in pump mode is a lot thinner than what it would be for a RPT designed for industrial use. For industrial RPTs and centrifugal pumps in general the inlet of the blade is thicker in order to avoid and endure cavitation. The relation between the

simulations could therefore differ from these simulations if another RPT model was used.

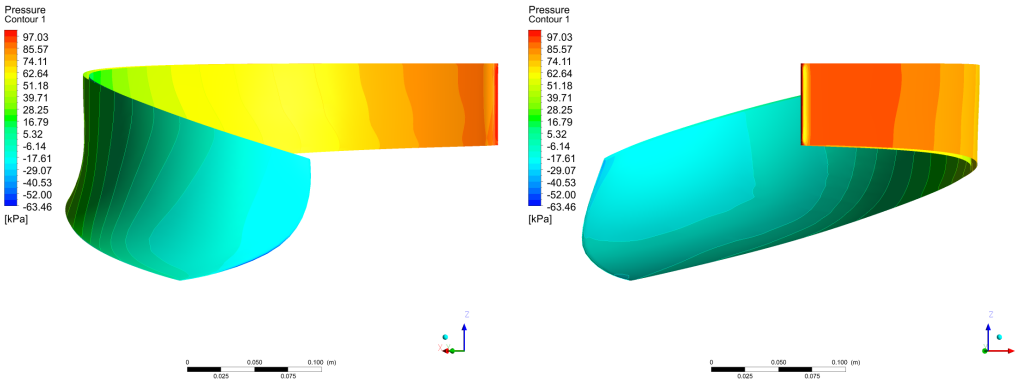

(a) Pressure side. **(b)** Suction side.

Figure 4.4: Pressure contours on the blade when $c_{m0} = 1.36199 m/s$ and $c_{u0} = 0 m/s$.

Figure 4.4 show the pressure and suction side of the blade for volume flow at BEP and no imposed pre-rotation. It is evident that the low-pressure area is larger on the suction side than on the pressure side, as expected. As discussed in section 2.2 it is desirable to decrease this pressure difference. The area of the low-pressure zones on the pressure and suction side is unfortunately not evaluated separately in this master's thesis, only the total area is evaluated.

To evaluate the development of the flow at the inlet, pressure contours and velocity contours are studied. Figure 4.5, Figure 4.6 and Figure 4.7 show the pressure contour plots for low volume flow, the volume flow at BEP, and high volume flow, respectively. Figure 4.8, Figure 4.9, and Figure 4.10 show the velocity contour plots for low volume flow, the volume flow at BEP, and high volume flow, respectively. The contour plot at the top shows the contours at the inlet and the contour plot at the bottom in each figure shows the contours at the connection between the original domain and the extended inlet. Both the contours at the connection side 1 & 2 are included in order to visualize any differences between them. In all the figures the simulation with no pre-rotation is compared to simulation 15, the simulation with the most imposed pre-rotation apart from the test simulation. The pressure ranges in Figure 4.5, 4.6, and 4.7 are different, as shown by Table 4.1. Table 4.2 shows the velocity range for the Figure 4.8, 4.9, and 4.10.

Table 4.1: Maximum and minimum values of the pressure ranges in figure 4.5, 4.6 and 4.7.

Figure	Max [kPa]	Min [kPa]
4.5	-24	-56
4.6	-10	-35
4.7	-7	-20

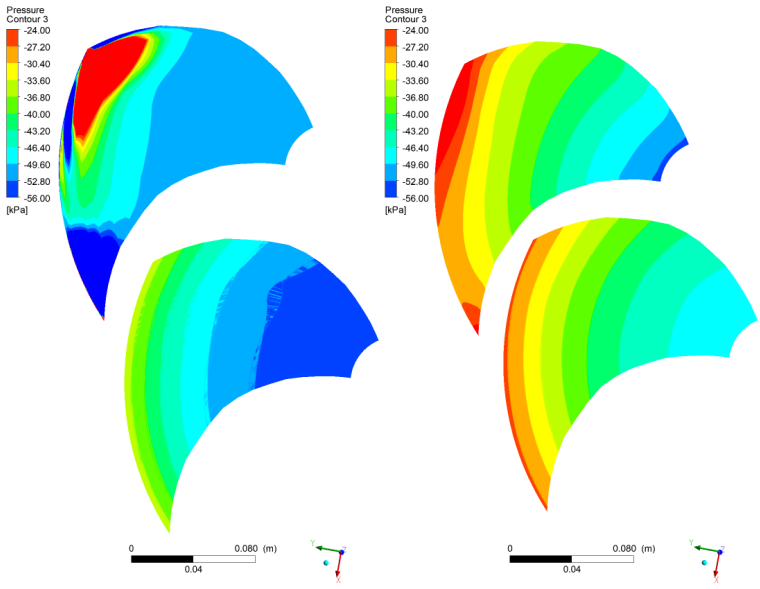

Figure 4.5: Contour plot of the pressure at the inlet and at the connection for $c_{m0} = 0.650301 m/s$. Left: $c_{u0} = 0 m/s$. Right: $c_{u0} = -8.62073 m/s$..

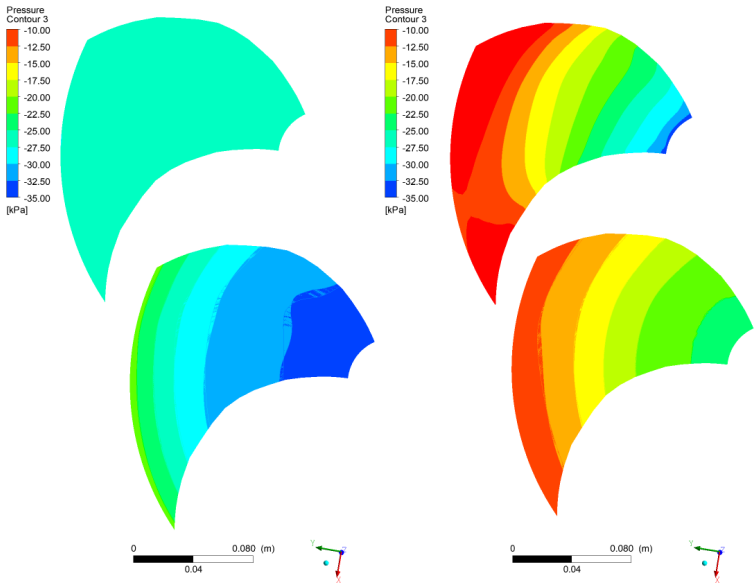

Figure 4.6: Contour plot of the pressure at the inlet and at the connection for $c_{m0} = 1.36199 m/s$. Left: $c_{u0} = 0 m/s$. Right: $c_{u0} = -6.04613 m/s$.

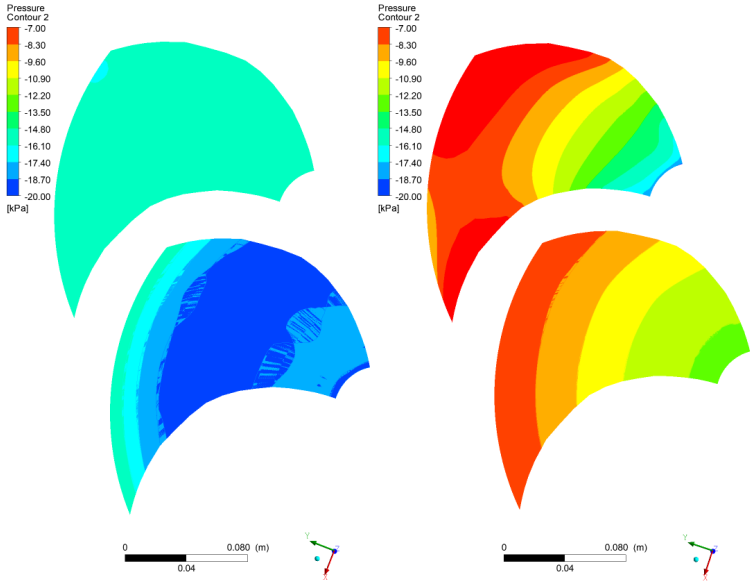

Figure 4.7: Contour plot of the pressure at the inlet and at the connection for $c_{m0} = 1.88274 m/s$. Left: $c_{u0} = 0 m/s$. Right: $c_{u0} = -3.29168 m/s$.

The transition from connection side 1 to connection side 2 is not completely smooth as there is a difference in the two contour plots at the connection, visualized in the lower plots in Figure 4.5, 4.6 and 4.7. However, the difference is not very big and it also seems to decrease when more pre-rotation is imposed as there is almost no difference in the contour plots at the connection for simulation 15 for all the volume flows.

As expected from Equation 2.5, the pressure increases in radial direction. The flow pattern is approximately the pattern of a solid body rotation and the pressure increases because of the centrifugal acceleration. The pattern is clear for all the simulations at the connection where the flow has developed from the initial conditions.

Table 4.2: Maximum and minimum values of the velocity ranges in figure 4.8, 4.9 and 4.10.

Figure	Max [m/s]	Min [m/s]
4.8	10.5	0.5
4.9	10.5	0.5
4.10	10.5	1.4

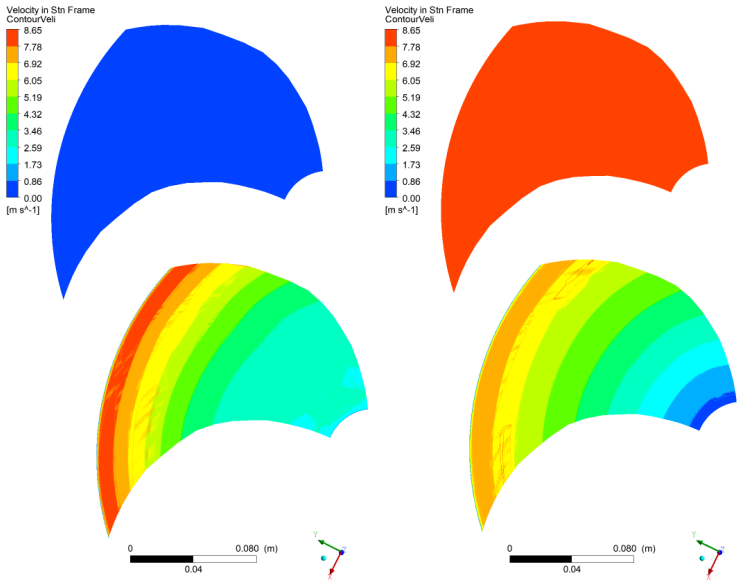

Figure 4.8: Contour plot of the absolute velocity at the inlet and at the connection for $c_{m0} = 0.650301m/s$. Left: $c_{u0} = 0m/s$. Right: $c_{u0} = -8.62073m/s$..

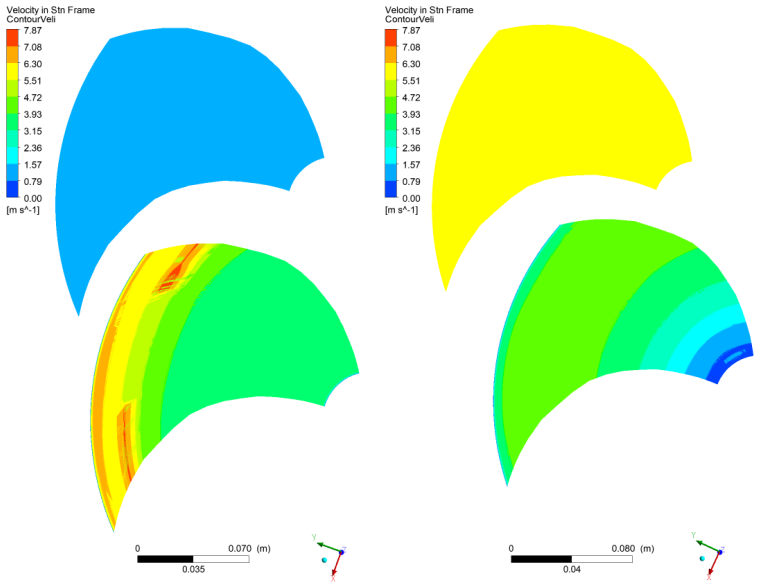

Figure 4.9: Contour plot of the absolute velocity at the inlet and at the connection for $c_{m0} = 1.36199 m/s$. Left: $c_{u0} = 0 m/s$. Right: $c_{u0} = -6.04613 m/s$.

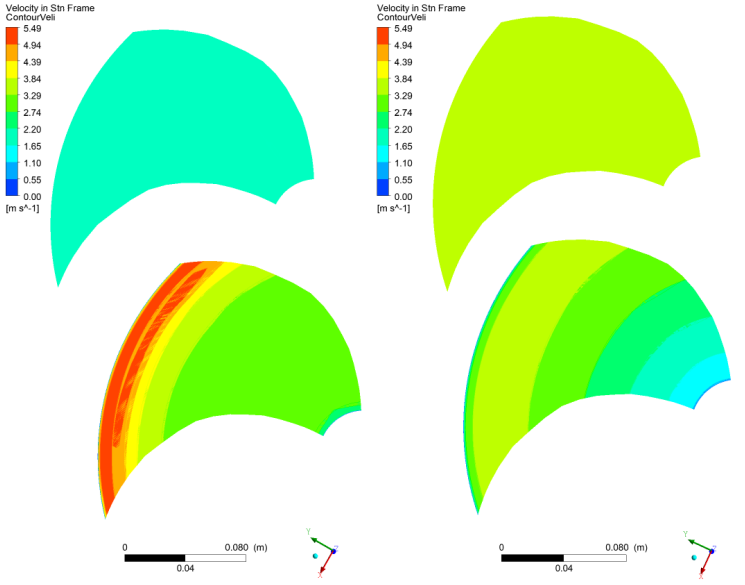

Figure 4.10: Contour plot of the absolute velocity at the inlet and at the connection for $c_{m0} = 1.88274 m/s$. Left: $c_{u0} = 0 m/s$. Right: $c_{u0} = -3.29168 m/s$.

From the velocity contour plots, Figure 4.8, 4.9, and 4.10, it is also evident that the connection has a minor impact on the flow. The velocity at the connection increases radially but close to the wall it decreases again. This is expected and caused by the no-slip wall boundary condition, as discussed in section 2.3.

The absolute velocity is constant over the whole inlet in Figure 4.8, 4.9, and 4.10, and the magnitude of the absolute velocity corresponds to the magnitude of the imposed pre-rotation. It is however not imposed as a rotating velocity component, but simply as a constant velocity in x-direction. Since the flow is bounded by the tube it will start to rotate right downstream of the inlet, but the magnitude of the rotational velocity component will change as the flow adjusts to the geometry of the tube.

The rotational component of the flow at the inlet should be implemented differently to avoid the need for adjustment. Then again, the rotational component would change from the inlet of the domain to the inlet of the blade anyway as the flow does not rotate as a perfect solid body in the inlet part of the domain. The rotational velocity is still higher for simulation 15 than for simulation 6 and 1, so the effect of the imposed pre-rotation can still be evaluated even though the actual rotational velocity component of the flow is unknown.

Chapter 5

Conclusion

The results from the CFD simulations conducted in this master thesis suggest that an imposed pre-rotation in the flow at the inlet of a reversible pump turbine decreases the area of the low pressure zone on the blade. This decreases the submergence needed in order to avoid cavitation. Although the simulations suggests that a larger imposed pre-rotation results in a smaller low pressure zone on the blade, the actual magnitude of the imposed pre-rotation is unknown. This is because the actual rotational component of the flow is unknown as it is wrongly implemented and since it develops while it approaches the blade from the inlet of the domain. As the total efficiency between the inlet and the outlet and the energy required to impose the pre-rotation is not taken into consideration in this master thesis, the ideal pre-rotation is not found.

Chapter 6

Further Work

A mesh refinement study should be conducted in order to decide whether the mesh is fine enough for the simulations to converge towards results that can be trusted. If the results of the simulations in the mesh refinement study is consistent with the results in this master thesis, the mesh is good enough. Otherwise, these simulations have to be discarded.

Simulations where the rotational component of the inlet velocity is implemented correctly should be conducted. The results from these simulations would be more trustworthy and also more helpful in order to investigate how large impact an imposed pre-rotation actually has. The same goes for the domain pressure. If the simulation pressure was physical it would be possible to evaluate the actual impact of every magnitude of the imposed pre-rotation and not just the trend.

Investigate the flow angle as the flow hits the blade and if there is a direct connection between the flow angle and the size of the low-pressure regions.

It would be interesting to evaluate the efficiency of the whole system in order to find the ideal imposed pre-rotation. The energy it takes to impose pre-rotation of various magnitudes has to be known if this is to be investigated.

In this master thesis the area of the low pressure zones on the whole impeller was evaluated. For further work the low pressure zones at the pressure and the suction side of the impeller could be evaluated separately. It would then be possible to investigate whether the total area of the low pressure zones on the impeller decreased because the pressure difference on the pressure side and the suction side of the impeller decreased, as discussed in section 2.2.

Simulations on the whole RPT and not just the impeller can be conducted for more accurate results.

Bibliography

[1] Billdal, Jan Tore, V. A., 2007. Recent experiences with single stage reversible pump turbines in ge energys hydro business.

[2] Brekke, H., 2000. Grunnkurs i hydrauliske Strømningsmaskiner. Vannkraftlaboratoriet, NTNU.

[3] Brekke, H., 2003. Pumper & Turbiner. Vannkraftlaboratoriet, NTNU.

[4] Cengel, Yunus A., C. J. M., 2010. Fluid Mechanics Fundamentals and Applications, 2nd Edition. McGraw-Hill.

[5] El Samanody, M.A., G. A. M. M. A. F., 2014. Investigations on the performance of centrifugal pumps in conjunction with inducers. Ain Shams Engineering Journal 5.

[6] Fukada, Toshiaki, T. S. K. T., 2014. Effects of curvature and vorticity in rotating flows on hydrodynamic forces acting on a sphere. International Journal of Multiphase Flow 58.

[7] Menter, F. R., 1994. Two-equation eddy-viscosity turbulence models for engineering applications. AIAA 32 (8).

[8] Olimstad, G., 2012. Characteristics of reversible-pump turbines. Ph.D. thesis, NTNU, Trondheim.

[9] Olimstad, Grunde, N. T. B. B., 2011. Design of a reversible pump-turbine - with purpose to investigate stability. 4-th International Meeting on Cavitation and Dynamic Problems in Hydraulic Machinery and Systems.

[10] Stepanoff, A. J., 1957. Centrifugal and Axial Flow Pumps, 2nd Edition. Krieger Publishing Company.

[11] Stranna, A., 2013. Testing of RTP in pumping mode of operation. Master thesis, NTNU, Trondheim.

[12] Svarstad, M. F., June 2013. Pumpe og turbinkarakteristikker i fire kvadranter. Project thesis, NTNU, Trondheim.

[13] Torød, K. M., December 2017. Simulation of pre-rotation at inlet flow of a pump turbine. Project thesis, NTNU, Trondheim.

Appendix A

Paper - 8^{th}International symposium on Current Research in Hydraulic Turbines

Simulation of pre-rotation in the flow at the inlet of a reversible pump turbine

Kristin Morvik Torød and Pål-Tore Storli

Department of Energy and Process Engineering,
Norwegian University of Science and Technology, Trondheim, Norway

E-mail: kristmt@stud.ntnu.no

Abstract. A reversible pump turbine (RPT) is a combination between a Francis turbine and a centrifugal pump and can therefore operate as both a turbine and a pump. RPT's can play an important role in stabilizing the electric power system in the future, as new intermittent energy sources constitute a larger and larger part of the energy mixture. A limiting factor for operation of a RPT is cavitation. To avoid cavitation the units must be submerged, which is an expensive action. This paper presents the preliminary work of a master thesis written at NTNU. The objective of the thesis is to conduct an investigation of the effect of pre-rotation with respect to characteristics and cavitation. Adding a rotation to the flow before it enters the inlet of the runner (pre-rotation) might be an effective countermeasure for cavitation, reducing the necessary submergence. Pre-rotation might also change the pump characteristic curves, indicating that it can be used to control the operation of the pump. The simulations are carried out using ANSYS CFX.

1. Introduction

A reversible pump turbine (RPT) is a combination between a Francis turbine and a centrifugal pump and can therefore operate both as a turbine and a pump [1]. RPT's can play an important role in the future of hydropower. As new intermittent energy sources constitute a larger and larger part of the energy mixture it is crucial to stabilize the electric power system. Pumped hydro storage power plants are an efficient solution as they can boost production (turbine) or consumption (pump) in peak power situations and deliver long term energy storage, depending on reservoir size [2].

A limiting factor for operation of a RPT is cavitation. In a pump the local pressure can fall below the vapour pressure for the pumped liquid. When this happens bubbles of vapour, called cavitation bubbles, will appear. This will typically occur on the suction side of the impeller blades where the pressure is lowest. The cavitation bubbles are then transported with the flow to regions with higher pressure which causes the bubbles to collapse. It is the collapse of cavitation bubbles that are undesirable as it causes vibration, noise, reduction in efficiency and damage to the impeller blades, [3].

To avoid cavitation the local pressure everywhere inside the pump must be above the vapour pressure. This is ensured by submerging the pump below the required Net Positive Suction Head, $NPSH_r$. $NPSH_r$ is defined as the minimum $NPSH$ necessary to avoid cavitation in the pump, [3], where $NPSH$ is defined as the difference between the inlet stagnation pressure head in the pump and the vapour pressure head.

$NPSH_r$ is lowest when the pump works at design conditions, and increases for operational points further away from the design point, as shown by the lowest graph in figure 1. It is therefore preferable to investigate how to decrease $NPSH_r$ at off-design conditions in order to extend the operational range for the pump. Such a decrease will straighten and extend the bottom part of the submergence graph. It is assumed that the reason for the rapid increase in $NPSH_r$ is that the difference between the inlet flow angle and the geometry of the impeller becomes so big that local low-pressure areas occurs. The objective of this paper is to conduct an investigation of the effect of pre-rotation with respect to cavitation. Adding a rotation to the flow before it enters the inlet of the runner might be an effective countermeasure for cavitation, reducing the necessary submergence. The rationale for this is explained in section 2.2.

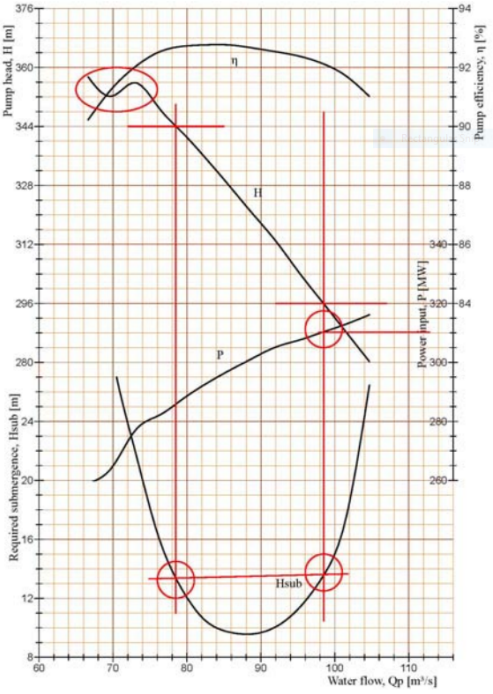

Figure 1. Pump performance diagram with critical points, [4].

2. Theory

2.1. Velocity triangles

The velocity triangles in Figure 2 shows the correlation between the velocity components at the inlet and outlet of a RPT. $c_{u1} = 0$ for a centrifugal pump with no pre-rotation at the inlet flow.

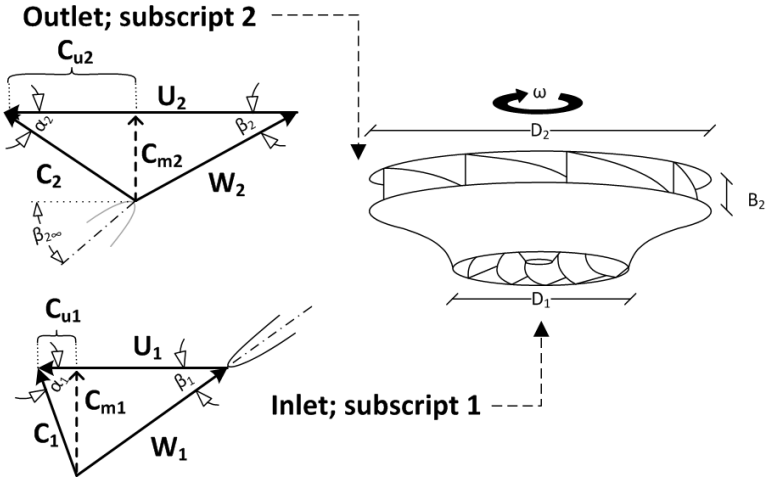

Figure 2. Velocity triangles at the inlet and outlet of a RPT.

2.2. Pre-rotation

When pre-rotation is imposed upon the inlet flow of the impeller c_{u1} is no longer zero. Stepanoff, [6], gives that the relative inlet head can be written in terms of the last part of Euler's head equation, as shown in equation 1.

$$H_1 = \frac{u_1 c_{u1}}{g} \tag{1}$$

By using the geometrical correlation between the velocity components from equation 2, equation 3 can be obtained. When the inlet flow angle, α_1, and the volume flow, Q, is known H_1 can be computed as β_1 is a constant and $c_{m1} = \frac{Q}{A_1}$.

$$c_{u1} = u_1 - w_{u1} = u_1 - \frac{c_{m1}}{\tan \beta_1} \tag{2}$$

$$H_1 = \frac{u_1^2}{g} - \frac{u_1 c_{m1}}{\tan \beta_1} \tag{3}$$

For a pump with no pre-rotation H_1 will be zero, while it will be positive for $\alpha_1 < 90^o$ and negative for $\alpha_1 > 90^o$. Inlet velocity triangles for the impeller with varying α_1-values are shown in Figure 3. When Q is kept constant, c_{m1} will be constant and a varying α_1 will only affect c_{u1}. Figure 3 describes velocity diagrams for flows with equal rotational speed, u_1, and varying α_1.

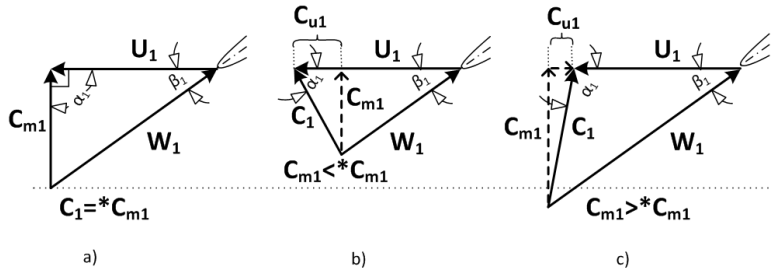

Figure 3. Inlet velocity triangles for a centrifugal pump.

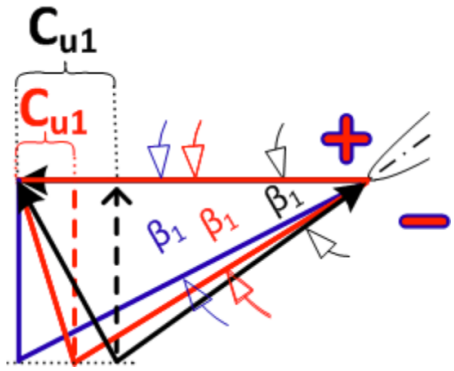

Figure 4. Inlet velocity triangles with varying c_{u1}.

The velocity triangles in figure 3 shows the size and direction of the velocity components as the flow hits the impeller. In both Figure 3a), 3b) and 3c) the relative velocity is perfectly aligned with the direction of the impeller blade. In reality the direction of the relative velocity will differ from the direction of the blade.

For a discharge smaller than the design discharge, as in Figure 3b) and the black triangle in Figure 4, the flow must have a certain rotational component in order to align perfectly with the direction of the blade. If there is no device in front of the inlet adding the necessary angular momentum to the flow to obtain this rotational component the flow will approach the inlet with $\alpha_1 = 90^o$, like the blue triangle in Figure 4. This causes a mismatch between the flow angle and the blade angle and creates a higher pressure on one side of the blade and a lower pressure on the other side of the blade, indicated by the large blue plus and minus signs.

When the flow approaches the inlet this pressure difference gives momentum to the fluid, which results in a rotational component of the flow. This reduces the mismatch between the flow angle and the blade angle and the pressure difference is reduced. However, the rotational component will never be as big as it needs to be to make the flow angle align perfectly with the blade angle (black triangle in Figure 4), because then the source of creating the rotational component in the first place is completely removed. The red velocity triangle in Figure 4 describes the direction of the flow where there is a balance between the rotational component caused by the pressure difference (red c_{u1}) and the remaining mismatch between flow angle and blade angle, causing the pressure difference itself (red plus/minus sign).

It is the presence of the low pressure region that can initialize cavitation, if the pressure is

low enough. This is the reason an imposed pre-rotation in the flow at the inlet is believed to counteract the formation of low pressure regions, it might cause the velocity triangle to shift towards the black velocity triangles in Figure 3 and 4.

2.3. Experimental data

The waterpower laboratory at NTNU has a RPT designed by Olimstad [2]. Stranna [7] have performed measurements on Olimstad's RPT in pumping mode which lays the ground for some of the analysis discussed in this paper. In Table 1 the geometrical constants for the RPT is presented. In addition, the gravitational constant, g, is set to be $9.81 m^2/s$.

Table 1. Known constant properties for Olimstad's RPT.

Constant	$D_1[m]$	$D_2[m]$	$B_2[m]$	$\beta_1[degree]$	$\beta_{2\infty}[degree]$
Value	0.349	0.3605	0.0587	12.8	12.02

From Stranna's measurements the volume flow, Q, the hydraulic head, H, and the efficiency, η, is extracted for different values of the rotational speed, n. There are data sets for 10 different n-values, and data for 15-19 different volume flows have been measured for each n-value. For every Q there exists 43 individual data sets.

First the average values for each Q for all the different n-values are calculated. Then the peripheral outlet velocity, u_2 and the absolute velocity in u-direction, $c_{u2\infty}$, can be calculated for the different volume flows and rotational speeds. c_{m1} and c_{m2} can be calculated as $c_m = \frac{Q}{A}$ and $c_m = c_{m\infty}$.

3. Model Description

3.1. Domain

To investigate how an imposed pre-rotation affects the characteristics and cavitational properties of a reversible pump-turbine, CDF simulations on the RPT impeller designed by Olimstad are performed in ANSYS CFX. The meshed impeller domain is shown in figure 5. The impeller domain is split in three parts, the inlet part, the blade part and the outlet part. This is visualized in figure 6 where the inlet and outlet part of the domain are meshed and the blade part is not. The domain is a rotating fluid domain with water as the defined fluid and a rotational velocity of 560 rpm. The water is further defined as a continuous and non-buoyant fluid, it is set to be isothermal with a temperature of 298.15K and the reference pressure for the domain is 0Pa.

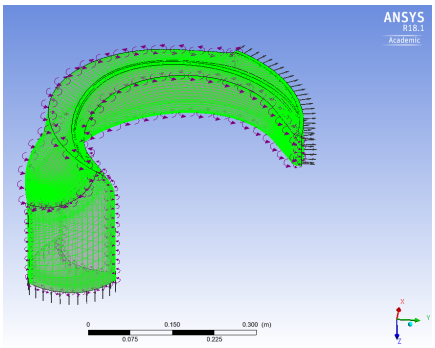

Figure 5. Meshed RPT impeller domain.

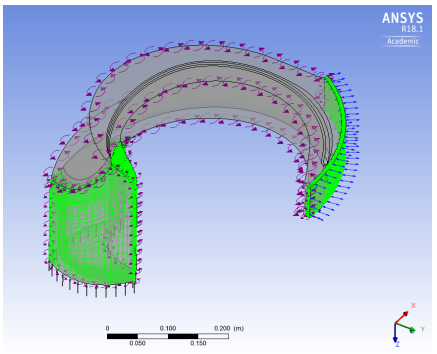

Figure 6. Meshed inlet and outlet part of domain of RPT impeller.

3.2. Boundary conditions

For this geometry there are a set of different boundary conditions. A smooth no-slip wall boundary is imposed on the blade as well as on the hub and the shroud. The hub and shroud in the blade part of the domain is rotating with the blade, but the upstream and downstream part of the hub and the shroud, the parts that belong to the inlet and outlet part of the domain, are not rotating. Since the whole domain is defined as rotating, the upstream and downstream part of the hub and the shroud are defined as counter rotating in order to represent stationary walls.

An outlet boundary type is imposed on the outlet of the domain. The flow regime is subsonic, and the boundary condition for mass and momentum is *Mass Flow Rate*. The imposed mass flow rate is $21.65kg/s$ for all the simulations. This is the mass flow rate for BEP when $n = 560rpm$, according to Stranna's measurements.

The inlet has an inlet boundary type with a subsonic flow regime. A *Static Pressure* boundary condition is imposed as the boundary condition for mass and momentum. Since Q is constant in all the simulations, c_{m1} is also kept constant. To investigate whether a change in the pheripheral velocity will have an impact on the cavitational properties a varying c_{u0}-value is imposed on the inlet. Each c_{u0}-value corresponds to an arbitrarily chosen α_0-value. Subscript 0 denotes the flow at the inlet of the domain, while subscript 1 denotes the flow at the inlet of the impeller. Stranna's measurements show that the inlet pressure will be 272kPa for an inlet flow with no rotation. The change in head, given by equation 3, for each value of α_0 is added to the inlet pressure and used as the static pressure boundary condition at the inlet.

The remaining boundary areas are imposed with a rotating boundary condition, as shown in figure 8. This is to imitate a simulation of the whole impeller and not just one blade.

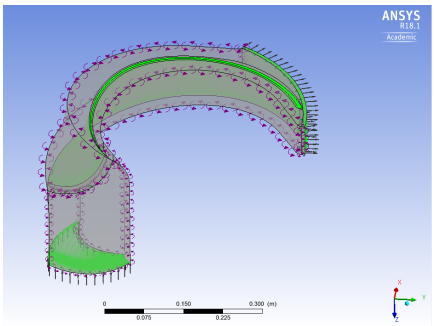

Figure 7. RPT runner domain with mesh on the inlet, outlet and blade

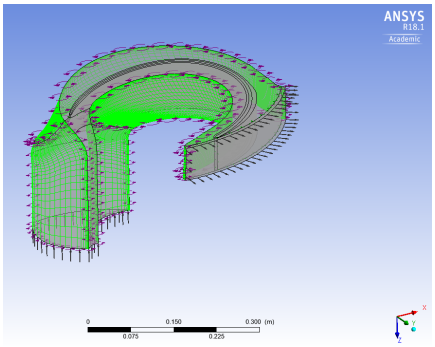

Figure 8. RPT impeller domain with mesh on the sides with a rotating boundary condition.

Table 2 presents the different values for α_0 imposed on the inlet flow and the corresponding change in c_{u0}, H_0 and p_0. For $\alpha_0 = 90^o$, $u_0 = 5.9948m/s$, $c_{m0} = 1.362m/s$, $H_0 = 0m$ and $p_0 = 272kPa$.

Table 2. Change in the inlet conditions for different values of α_0.

$\alpha_0[degree]$	$\Delta c_{u0}[m/s]$	$\Delta H_0[m]$	$\Delta p_0[Pa]$
70	0.4957	0.3652	3211.1
80	0.2402	0.1700	1494.4
85	0.1192	0.0827	727.1
90	0	0	0
95	-0.1192	-0.0795	-698.7
100	-0.2402	-0.1569	-1379.2
110	-0.4957	-0.3094	-2720.6

To find the initial values at the inlet the values from table 2 were added to the inlet values for $\alpha_0 = 90^o$, given by Stranna.

3.3. Turbulence model

The SST model is a simple and widely used turbulence model for turbomachinery simulations. Although the model is a combination of the best parts of the $k-\omega$-model and the $k-\epsilon$-model it is not able to give a completely accurate description of what is happening. For more accurate results LES (large eddy simulations) or DNS (direct numerical simulations) can be conducted, but those kind of simulations are extremely expensive and therefore avoided if the results given by using a turbulence model are good enough.

3.4. Mesh

The impeller which was the subject of the CFD simulations in this report was provided as a pre-meshed .cgns file without any possibilities of changing the mesh. A mesh refinement study

was therefore not conducted. The mesh consists of 322048 hexahedrons and have 347556 nodes. A mesh refinement study reveals whether a mesh is fine enough or not, and since no such study was carried out, the simulations, in the worst case scenario, might be completely off.

3.5. Steady state

As no attention is paid to pulsations of any kind only steady state simulations are performed. A steady state simulation is only reliable once it has converged, and the result are not time dependent. Due to the lack of time dependency no time step can be defined and no time step refinement study has to be conducted.

3.6. Convergence

The convergence criterion for the simulations were set to be of max residual type with a residual target of 0.001. This criterion were never met for any of the simulations and they were all stopped after 300 iterations. As the rotating speed of the impeller was 560 rpm and the physical timescale was 1/560, 300 iterations corresponds to 5 rotations. The RMS-values for mass and momentum did not converge towards one constant value, but fluctuated periodically. When the simulations went on for 1120 iterations the periodical pattern became clearer, as shown in figure 9. Since the fluctuations remained when the number of iterations were increased, 300 iterations were deemed sufficient.

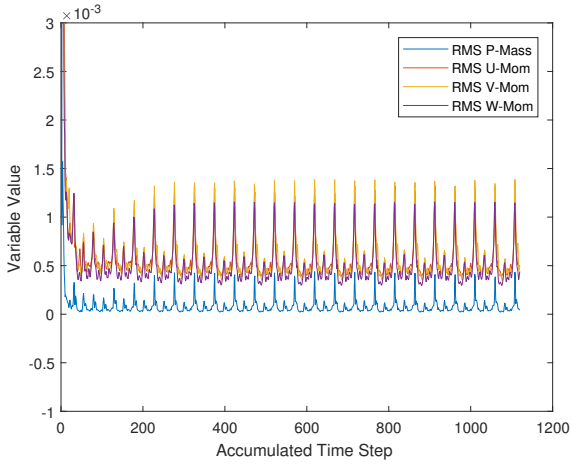

Figure 9. Convergence of the RMS-values for mass and momentum when there is no imposed pre-rotation.

3.7. Mass conservation

Mass conservation were checked by comparing the mass flow at the outlet and the inlet. The error was estimated to be below 0.3% for all the simulations.

3.8. Smooth wall

A smooth wall condition were imposed on the no-slip blade in the simulations. This can contribute to a less accurate description of the real model as the impeller does have a wall roughness. However, as the objective of this part of the report is to investigate the relative

change in low pressure zones for an inlet flow with a variation of imposed pre-rotations, the smooth wall assumption may be harmless as the simulations can be compared with each other as long as they are defined in the same way.

3.9. Walls on the inlet part of the domain

On the inlet part of the domain two walls were defined. The outer wall is forming the wall boundary the water is flowing within, while the inner wall boundary implies that the shaft the runner is rotating around is extended further down in the inlet of the RPT. This can be a bit problematic as this is not the case for the real model and can therefore lead to inaccuracies in the simulations.

4. Results

All the simulations presented in section 3 resulted in a nonphysical negative pressure on the inlet of the impeller. New simulations with a reference pressure of $100MPa$ for the domain and an inlet pressure corresponding only to the pressure changes presented in table 2 were conducted, but the negative pressure zone were even bigger for these simulations. Even if the initial simulations (the simulations with 0Pa as reference pressure) were expected to have a strictly physical behaviour as all the imposed boundary conditions were given by experimental measurements, the effect of a change in the pheripheral velocity can still be evaluated. As a result of the nonphysical behaviour multiple pressure zones on the blade were investigated for all the simulations, not only the pressure zones with a pressure less than the vaporization pressure for water at 25 degrees. The size of the affected area was compared for the different simulations. Figure 10 shows the area of the pressure zones as a function of pressure, the whole area of the blade is $0.1222m^2$.

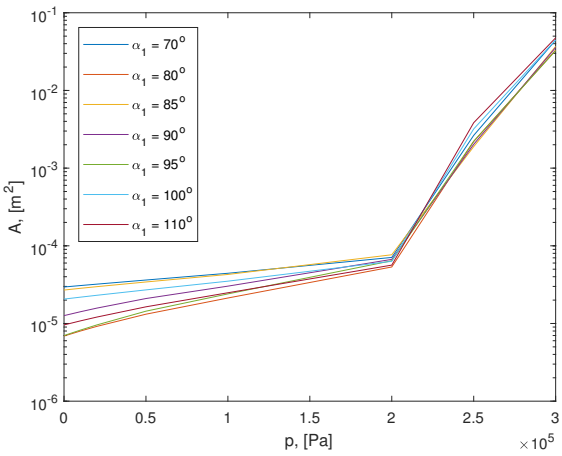

Figure 10. Area of the pressure zones on the blade for different α_0.

No clear connection between α_0 and the the size of the area exposed to a risk of cavitation was found. The conducted simulations for $\alpha_0 = 80^o$, 95^o and 110^o had a lower risk of cavitation, while $\alpha_0 = 70^o$, 85^o and 100^o had a higher risk of cavitation than $\alpha_0 = 90^o$.

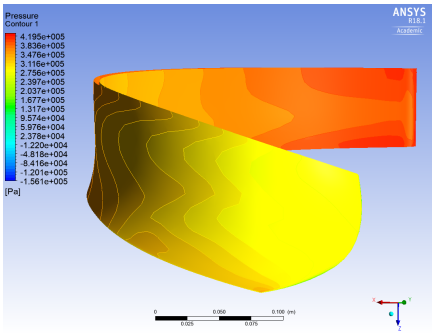

Figure 11. Pressure at the pressure side of the inlet of the impeller for $\alpha_0 = 90^o$.

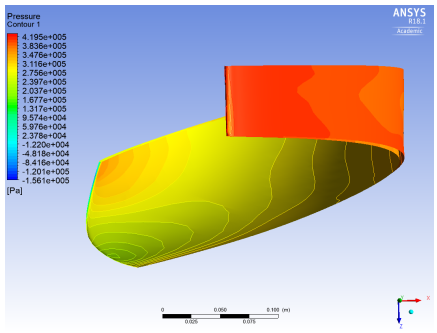

Figure 12. Pressure at the suction side of the inlet of the impeller for $\alpha_0 = 90^o$.

Figure 11 shows the pressure side of the impeller for inlet flow with no pre-rotation and figure 12 shows the suction side of the impeller for inlet flow with no pre-rotation. For a flow at the inlet with no pre-rotation the low pressure zone on the suction side covers a bigger area than on the pressure side. Changing the α_0-value did not seem to have an appreciable affect on the relation between the low pressure zones at the pressure and suction side of the blade.

Even if the negative pressure zones at the inlet of the impeller are nonphysical, it does not mean that the whole simulation is nonphysical. In fact, the negative pressure zones were almost expected. The inlet of the RPT impeller is very thin, a lot thinner than for a centrifugal pump. Impellers usually have a thicker inlet in order to avoid cavitation, i.e. low pressure zones. A thinner inlet results in zones with lower pressure, and the thin inlet can also cause problems when it comes to solving the system equations correctly. A thin inlet requires a very fine mesh, otherwise the results can be wrong in that area.

5. Conclusion

The need for submergence of the RPT increases rapidly for volume flows that deviates form the volume flow at BEP. Changing the peripheral velocity did not seem to have an impact on the cavitation. However, the results found in this paper are not enough to dismiss the hypothesis as the number of simulations are limited and only the volume flow for BEP is investigated.

6. Further work

First off, a mesh refinement study should be carried out in order to decide whether the conducted simulations are good enough. If the results of the simulations in the mesh refinement study is consistent with the results in this project report the used mesh good enough. Otherwise, these simulations have to be discarded.

Simulations with an imposed pre-rotation should be analyzed, not only simulations with a varying peripheral velocity.

Another important point is to study the effect of pre-rotation outside of BEP. As the goal is to decrease the risk of cavitation without further submergence the cases of highest importance are those exposed to a higher risk of cavitation.

Simulations on a geometry without a shaft in the inlet would possibly lead to more accurate results. Simulations on a geometry with an extended inlet can also be conducted in order to investigate how a more developed flow would affect the simulations. In addition, other methods of imposing pre-rotation to the flow could be investigated.

References

[1] Svarstad, M. F., june 2013. Pumpe og turbinkarakteristikker i fire kvadranter. project thesis, NTNU, Trondheim.

[2] Olimstad, G., 2012. Characteristics of reversible-pump turbines. Ph.D. thesis, NTNU,Trondheim.

[3] Cengel, Yunus A., C. J. M., 2010. Fluid Mechanics Fundamentals and Applications, 2ndEdition. McGraw-Hill

[4] Billdal, Jan Tore, V. A., 2007. Recent experiences with single stage reversible pump tur-bines in ge energys hydro business

[5] Brekke, H., 2000. Grunnkurs i hydrauliske Strømningsmaskiner. Vannkraftlaboratoriet,NTNU

[6] Stepanoff, A. J., 1957. Centrifugal and Axial Flow Pumps, 2nd Edition. Krieger PublishingCompany.

[7] Stranna, A., 2013. Testing of RTP in pumping mode of operation. master thesis, NTNU,Trondheim